IMPLEMENTATION OF GRID-FORMING MULTILEVEL CONVERTERS CONTROL BASED ON THE SMC-REACTIVE POWER SYNCHRONIZATION METHOD FOR RENEWABLE POWER PLANTS

K.Lokeswar Reddy[1], Dr. P. Sujatha[2]
[1]PG-Scholar, Department of EEE, JNTUA College of Engineering (Autonomous)
Ananthapuramu,India.
[2]Professor, Department of EEE, JNTUA College of Engineering (Autonomous)
Ananthapuramu,India.
lokeshreddykavalakuntla@gmail.com[1], psujatha1993@gmail.com[2]

Abstract
Synchronous generators (SGs) have been phased out of conventional power plants due to the rising use of renewable energy sources in the electrical sector. Electronic power converters are commonly used to connect renewable power plants to power grids, but their mode of operation means that they cannot match the power generation services provided by SGs. Grid-forming converters are an example of a novel type of electronic converter whose control strategies are meant to emulate the functionality of SGs (GFCs). To separate the synchronizing power from the active power control of a renewable generation source connected to a converter, we present a new GFC control technique based on the reactive power Synchronisation (RPS) method. This research accomplishes this by comparing and contrasting three widely used energy generation technologies: batteries, photovoltaic (PV) plants, and full-converter wind turbines. The paper suggests models and controls for all these factors, which have substantial impacts on the grid services provided by renewable energy facilities. The paper then proposes a GFC-RPS control system and shows how effective it is across a range of applications, such as inertial response, which provides instantaneous power via a fast frequency response after a grid has experienced a load variation. Wind turbines and energy storage devices can provide these services at any power output, while PV plants can only do so when operating at less than full capacity. The results of the study provide further evidence that the GFC-RPS control method is capable of keeping the AC voltage at the converter's output terminals at a constant value. The study concludes with an analysis of hot switching GFCs, a technique used to maintain supply during the switch from grid-connected to isolated-operation mode with a variable load. Results demonstrate that the proposed GFC-RPS control operates as a genuine voltage source and behaves like a conventional SG by maintaining a constant voltage and frequency. For the purpose of lowering harmonics and raising the time-speed response of the system, this paper employs a multi-level inverter and sliding mode control.

Keywords: Sliding mode control, converter hot swapping, quick frequency response, reactive power Synchronisation, and renewable energy sources all fall under the umbrella term, grid-

forming power converter.

I. INTRODUCTION

In this setting, grid-forming converters (GFCs) were originally introduced as an unique control mechanism for Multi-level Inverter operating as uninterruptible power supply to maintain load voltageand frequency when separated from micro grids [2, 3]. Since GFCs are low-impedance voltage sources,precise Synchronisation methods are required to allow them to run in parallel with other GFCs servingisolated loads.

GFC development has accelerated in recent years as more and more renewable energy sources have been integrated into grid infrastructure. Synchronous generators in conventional power plants are beingphased out in favour of electronic power converters as a means of interfacing renewable energy systemswith the grid. What this means is that SGs control the voltage and frequency of the electricity grid. Renewable generation covers a large percentage of energy demand (>70%) in many European electricalnetworks' present energy generation scenarios, and some governments have proposed that renewable generation fulfil 100% of total energy demand in the next decades [4]. In contrast to SGs, which producevoltage, grid-following converters produce current that is controlled by the grid's voltage. Grid services are governed by international grid codes [5], which establish criteria for the operation of renewable generation. voltage dip continuity, reactive voltage control, and power frequency regulation. Grid supporting occurs whenever a grid-following converter provides services after taking terminal voltageand frequency readings. A power-frequency (P/f) regulation service monitors frequency variations and responds by adjusting the amount of active power. SG governors are a model for this. Some studies [5,6] have found that grid instability can occur when these generators' inertial responses are emulated at high penetration rates of electronic converters.

Whenever there is an inequity in the distribution of power in an electrical network, the result is a frequency deviation. After a power outage, grid-following converters restore power by adjusting their output frequency to compensate for the difference. Converters operating in this mode will keep the frequency steady during synchronous generation, but they will not be able to fine-tune it. As a result, "anti-islanding" safeguards must be built into renewable power plants [6]. Economic downturns in GFCs frequently resemble SGs.

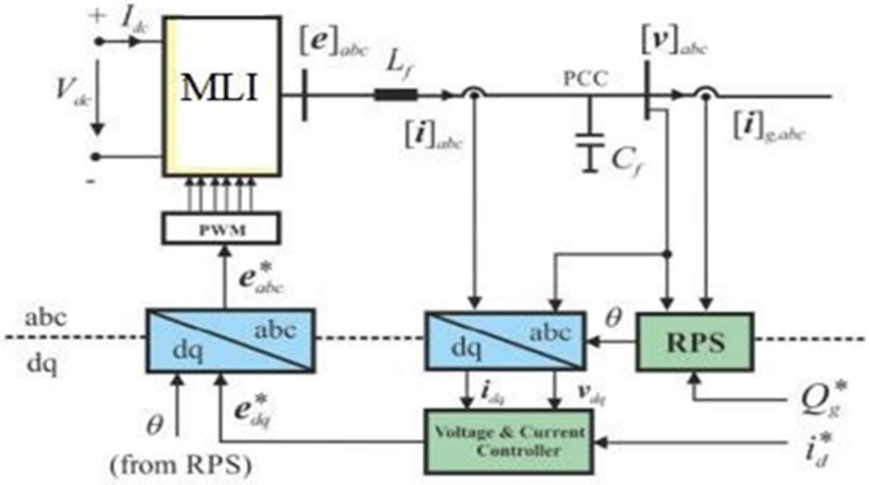

Figure.1: Grid-forming Multi Level Inverter system

II. METHODOLOGY

SYSTEM DESCRIPTION

A controlled voltage source electronic converter is shown in Fig. 1. The input current, I dc, and the terminal voltage, V dc, are both direct currents. An LC filter is connected to the converter. The GFC can be managed with I, V, and I g. Instantaneous active and reactive power are determined at the GFC's grid connection.

The GFC's operational mode is determined by the PCC-grid breaker. DC VSC plugs are compatible with green power sources. The three investigated DC sources are depicted in Fig. 1. Fig-2. Energy level is at 2a. A variable-speed wind generator with a full-converter back-end is depicted in Fig. 2b. The

photovoltaic power plant is depicted in Fig. 2c. The current drawn from a battery can be represented by I bat. The current through the converter (I fc) is different from the current through the photovoltaics (I PV).

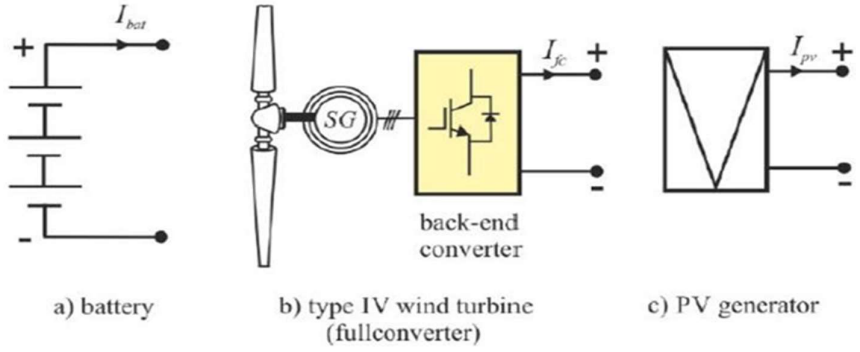

Figure.2: DC sources: a) battery, b) wind turbine, c) PV generator

REACTIVE POWER SYNCHRONIZATION BLOCK

As soon as the GFC begins active power transmission to the grid, Q g and are dynamically related. There won't be any fighting in this marriage. An illustration of the RPS block's reactive power syncing loop is shown in Figure 3. An angle, Q g*, and the GFC output reactive power, Q g, are obtained by multiplying the difference between the reactive powers of the reference source and the load by the synchronization constant, Ks, to obtain the per-unit-frequency-increase applied to the control.

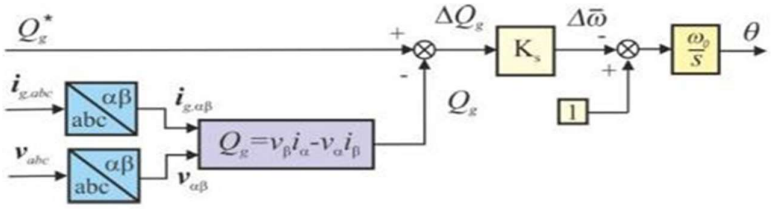

Figure.3: Reactive power synchronization loop

The GFC's instantaneous $[i]$,abc and $[v]abc$ values are normalized for use in the reactive power Calculation. At grid synchronization ,$Q_g^* = Q_g$ for reactive power and $Q_g^* \neq Q_g$ when the grid

frequency is not zero, Q g*- Q g corrects for it in the synchronization loop. In the event of a

main breaker failure, the GFC will be islanded because the $[i]$,abc vector currents will be zero. If ΔQg is zero, then the GFC load is fed at a frequency of ω_0. The RPS circuit does not conform to the voltage phase set by the PCC. It adjusts the synchronization frequency increase, $\Delta\omega$, after measuring reactive power. After the main breaker trips, the GFC can continue to function in islanded mode by adjusting the amplitude and frequency of the PCC voltage. By switching to grid mode, you can avoid this problem. When there is no control reference, the PLL measures the voltage angle when the circuit breaker trips

Ks is a synchronization constant used by by using the RPS control block to determine the difference in reactive power between the reference and generated systems, the frequency of the reference rotary system can be increased, Q g* and Qg. . To get from eq. (1). Transfer function (2) and the difference between Δp_g^* and $k_{p\delta}\Delta\delta$.

$$\frac{1}{\omega_0}\frac{d\delta}{dt} = \bar{\omega} - \bar{\omega}_g \quad (1)$$

$$G_{qp}(s) = \frac{\omega_0}{s+\frac{R_g}{L_g}\omega_0} \quad (2)$$

$$\Delta Qg = \frac{\omega_0}{s+\frac{R_g}{L_g}\omega_0}(\Delta p_g^* - k_{p\delta}\Delta\delta) \quad (3)$$

DC SOURCES MODELING AND CONTROL BATTERY MODEL

Figure 4 depicts the electrical model [43]- [45] of a battery, which consists of a voltage source, E b, which varies with the SoC indicator, a resistor in series (Rs), and a capacitor in parallel (Cb), with the resistance (Rp) representing the battery's transient capacity (or discharge rate). The voltage at the battery terminals, Vdc, responds slowly to transients in the battery current, Ib, rather than immediately, τb= RpCb.

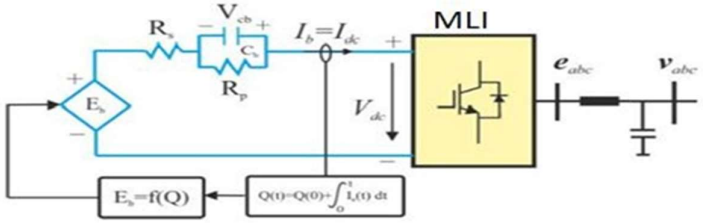

FIGURE 4. Equivalent circuit of a battery

Battery System-on-Chip (SoC) means.

$$S0C = 1 - \frac{Q(t)}{Q_n} \quad (4)$$

In this case, we can express the rate of discharge, Q (t), in terms of its nominal capacity, Q_n, by rewriting the expression:

$$Q(t) = Q(0) + \int_0^t I_b dt \quad (5)$$

E_b, the dependent voltage source expression, is computed by using the following formula.

$$E_b(t) = E_0 - K.\frac{Q_n}{Q_n - Q(t)} + Ae^{-BQ(t)} \quad (6)$$

The nominal no-load voltage, denoted by E_0, is the first term. The second term, with a minus sign after it, represents the voltage drop experienced by the cell during discharge and is denoted by the expression K/SoC. As can be seen in Fig. 5, this drop is most noticeable at the very end of the battery's discharge curve (SoC ~0). The third term, expressed as an exponential function, represents a model of when a battery is subjected to a surge during charging at SoC ~1.$Ae^{-B(t)}$.

Fig. 5 is a discharge curve, and the parameters that best describe it are listed in Table 1. (6).

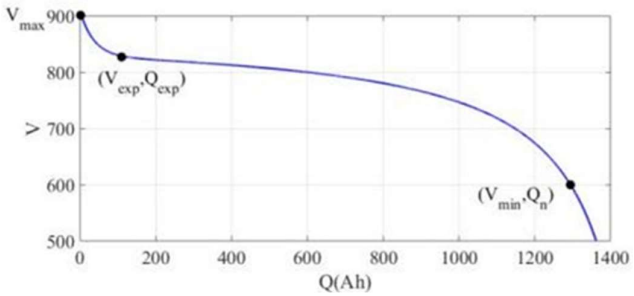

Figure.5: Discharge curve of the battery

Terminal voltage is calculated using a set of dynamic equations, Vdc, are

$$\frac{dV_{cb}}{dt} = \frac{-1}{C_b}\left(I_b + \frac{V_{cb}}{R_p}\right) \quad (7)$$

$$V_{dc} = E_b + V_{cb} - R_s I_b \quad (8)$$

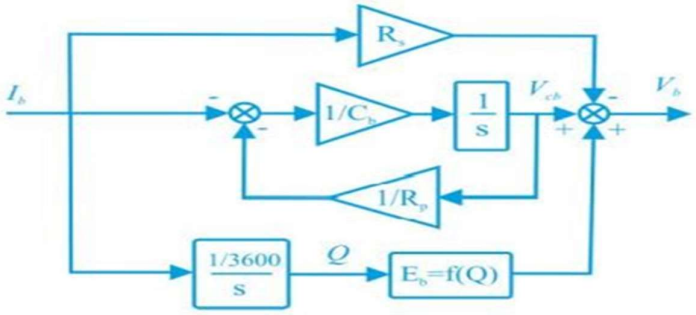

Figure.6: Battery block diagram

In Figure.6, we see a battery block diagram that uses Eqs. (4) and (5) to describe its internal workings (5). Since the battery's SoC exhibits only slight variation, Assuming the E b voltage to be stable.

if the evaluation window is narrow enough, the battery's dynamic response to shifting power set-point values and grid frequency variations can be assessed. In Fig. 5, Vn = 800 V represents the nominal voltage for a battery with a 600 Ah discharge capacity. SoC voltage variation is minimal, so discharging the battery at 1 C (1200 A) for several seconds causes little harm.

FULL-CONVERTER GENERATOR MODEL

The DC bus of a type-IV wind turbine is shown in Figure 2. (b). In a traditional FC setup, the rotational speed of the turbine is set by the torque instruction sent to the back-end converter. The q-axis current is proportional to the rotor torque when utilising a control mechanism that exploits the generator rotor's flux. It is usual practise to set the current in the d-axis to zero in order to produce a desirable torque from a low current. The generator's output DC voltage is regulated and maintained within the front-end converter. In contrast, the front-end converter of a GFC controls the power output of the wind turbine. The converter in the rear of the system maintains a steady DC voltage. The generator's active power is proportional to the regulator's output current I fc. Unlike conventional FC controls, which transfer active power straight to the turbine from the generator and front-end converter, this system reroutes active power before it reaches the turbine. A simplified electrical model of the FC turbine (type IV) is shown in

Figure 2; in this model, a DC voltage regulator's output represents a dependent current source (b). According to the voltage deviation, Ifc is determined, $edc = V_{dc}^{*} - V_{dc}$, as

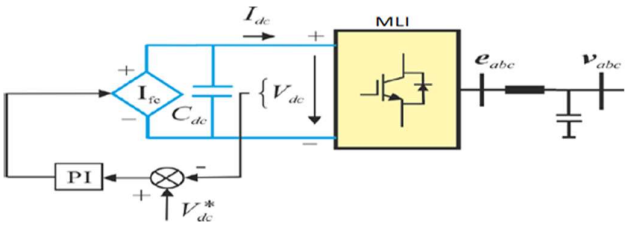

Figure.7: Front-end converter

$I_{fc} = K_{pv}e_{dc} + K_{PI}\int e_{dc}dt$ (9)

By solving a Capacitor's Changing Dynamic Equation, we can determine its voltage response, Vdc, Cdc

$$\frac{dV_{dc}}{dt} = \frac{1}{C_{dc}}(I_{fc} - I_{dc}) \quad (10)$$

With the voltage vector pointing toward the d axis of the rotary reference system and assuming no losses in the front-end converter, the following relationship is given by [49]:

$$I_{dc} = \frac{3}{4}m_a i_d \quad (11)$$

At the converter's output, the current vector has a direct component, denoted by i_d, and an amplitude modulation index, m_a.

PV GENERATOR MODEL

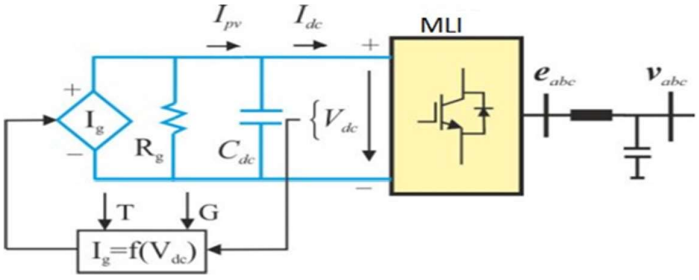

Figure.8: Solar energy generator equivalent circuit

The terms "source" (Ig) and "resistance" (Rg)

$$I_g = N_p I_i\left(\frac{R_{s,pv}}{R_{s,pv}+R_{p,pv}}\right) \quad (12)$$

$$R_g = \frac{N_s}{N_p}(R_{s,pv} + R_{p,pv}) \quad (13)$$

An ideal PV module has a series resistance of Rs,pv and a parallel resistance of Rp,pv. There are Ns strings, each of which is made up of Ns modules connected in series, and Np parallel strings, each of which is made up of Np modules connected in parallel. The formula for the terminal current of the module, Ii, is as follows.

$$I_i = I_{ph} - I_0\left[\exp\left(\left(\frac{R_{s,pv}}{R_{s,pv}+R_{p,pv}}\right)\frac{V_{pv}+R_s I_i}{KV_{sh}}\right) - 1\right] \quad (14)$$

Ipv = f (G, T), where Vpv is the voltage at the PV module's terminals and I pv is the current and G(W/m2) is the irradiance and T(°C) is the temperature. The short-circuit current of the PV module is very near to I0, where K is the ideality factor and V Th is the thermal voltage. In

Fig.9, we see the I(V) and P(V) curves for the PV generator under test. Assuming a maximum direct current voltage of Vdc,max= 700 V, we find that the maximum power, Pdc,ax, is 2 MW (point A).

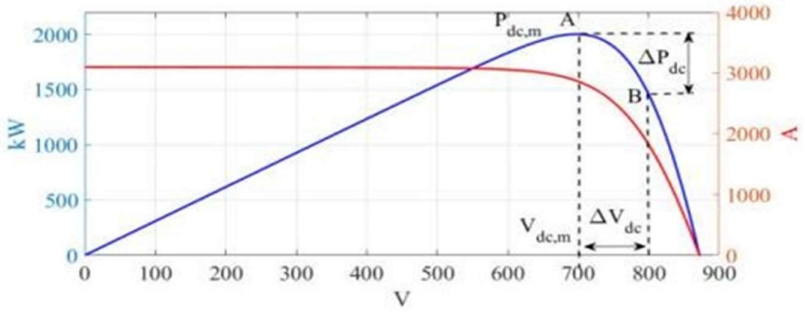

Figure.9: I(V) and P(V) curves of a PV generator

Sliding Mode Control

Sliding Mode Control's control law can be applied without first characterizing the disturbance waveform. SMC's main benefit is its resistance to random noise. Sliding Modes are a usual behavior in switching system. It is useful tool for controlling uncertain dynamical systems. It is a simple way of applying the Internal Model Principle by resorting to the Equivalent Control to retrieve some information about an uncertain system by low-pass filters. Sliding mode control is a simple yet effective technique for steering the paths of a dynamic system within the bounds of the sliding mode subspace, using nearly limitless gain. This lower-order sliding mode produces trajectories with beneficial properties (e.g., the system naturally slides along it until it comes to rest at a desired equilibrium). The resilience of sliding mode controls is its primary strength. Since there are only two possible outcomes, the control does not have to be extremely exact and is less likely to be affected by incoming parameter fluctuations (such as "on" and "off" or "forward" and "reverse"). In addition, the sliding mode may be achieved in a finite amount of time since the control rule is not a continuous function (i.e., better than asymptotic behavior). Sliding mode control describes the ideal controller for a large class of dynamic systems, although in some situations, bang-bang control is necessary for optimality.

Mathematical Description of Sliding mode control: -

Consider an example of one dimensional motion of unit mass which is pulled by control input force and resisted by the disturbance force which is given by the term f(x_1, x_2, t) where

$x1^{\cdot} = x2$ (15)

$x2^{\cdot} = U + f\,(x1, x2, t)$ (16)

Where disturbance is bounded disturbance and this disturbance has included the viscous friction force and unknown rigid forces.

$| f(x1, x2, t) | \leq L > 0$ (17)

The system states are x_1, x_2 where x_1 *is position and* x_2 is velocity To design a feedback control law U=U (x_1, x_2)

$\lim_{t \longrightarrow \infty} x_1, x_2 = 0$ (18)

$U = -k1x1 - k2x2 \quad , k1, k2 > 0$ (19)

It Provides the asymptotic stability only when disturbance is (x_1, x_2, t)=0 It drives the system

state to a bounded domain S for the given bounded disturbance f(k_1, k_2, L). It will converge the system to stability at equilibrium point. Let the desired compensated dynamics for the given system be

$x1^{\cdot} + Cx1 = 0$, $C > 0$ (20)

$x2(t) = x1^{\cdot}(t) = -Cx1(0)e^{-ct}$ (21)

System states x_1 ,$_2$ converges to equilibrium point asymptotically. No disturbance effect is observed on the system compensated dynamics. Here we introduce a new variable in the state space σ = σ (

$x1, x2$)

$\sigma = x_2 + Cx_1$ (22)

To achieve the asymptotic convergence of x_1, x_2 in presence of disturbance σ must be driven to zero in finite time by U. σ dynamics must include control law

dv/dt =-C $x_2 + u$ (23)

we assume that U=- C $x_2 + u$ (24)

now dv/dt < σL+συ (25)

selecting υ=-^{p}signum (σ)

consider V= ½ σ^2 (26)

$\sigma = \sqrt{2}V$ (27)

the final control law would be

U= -C$x2$ − ^{p}signum (σ) (28)

Actual Conditions for sliding mode Control

- ✓ System is stable confined to s=0
- ✓ Control moves states towards this stable sliding surface

SMC Design Methodology

- ➢ Design a sliding manifold or sliding surface in state space.
- ➢ Design a controller to reach the sliding surface in finite time.
- ➢ Design a control law to confine the desired state variables to the sliding manifold.

To achieve the desired trajectory of the state variables, SMC relies on the engineering behind the control law for a sliding surface. To adopt a switching function, the standard control law for a single-switch dc-dc converter is: u= ^{1} [1 + $sign(S)$] where u is

2

grid voltage is both the switching function (logic state) and the state variable of the converter's power switch. The grid voltage error is defined as the difference between the actual value and the reference value, and this difference forms the sliding function in the general sliding mode control theory, which is given by

S=$Vg, ctual - Vg, reference$ (29)

III RESULTS & DISCUSSION

Here, we show what happened when we applied the discussed control strategies to a simulated GFC converter. Switch s1 connects the GFC to the grid, and a local dynamic load is connected to the GFC locally, as shown in Fig. 23. (AC motor). The DC source can be anything from a

battery to an FC wind turbine to a PV power plant.

III. RESULTS AND DISCUSSIONS

Here, we show what happened when we applied the discussed control strategies to a simulated GFC converter. Switch s1 connects the GFC to the grid, and a local dynamic load is connected to the GFC locally, as shown in Fig. 23. (AC motor). The DC source can be anything from a battery to an FC wind turbine to a PV power plant.

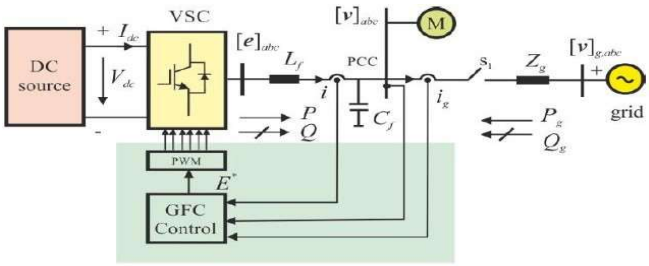

Figure 10: Block Diagram using VSC and PI Controller

Case 1: Frequency Response for a load change from 90 MW to 108 MW

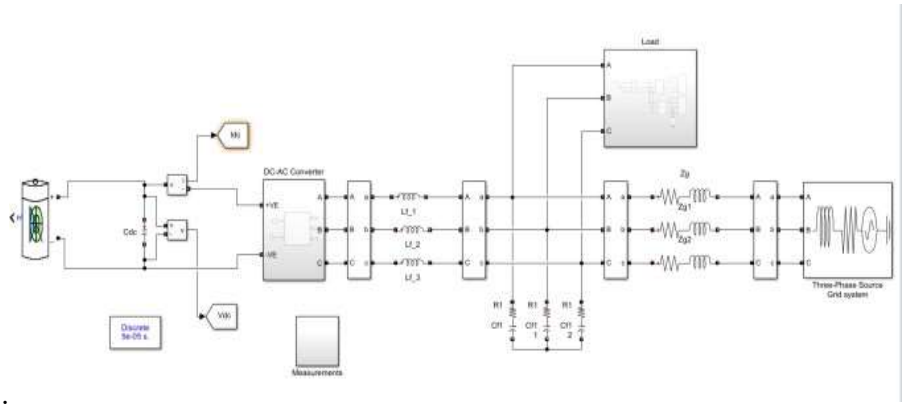

.

Figure 11: - Simulation Diagram For frequency response for battery

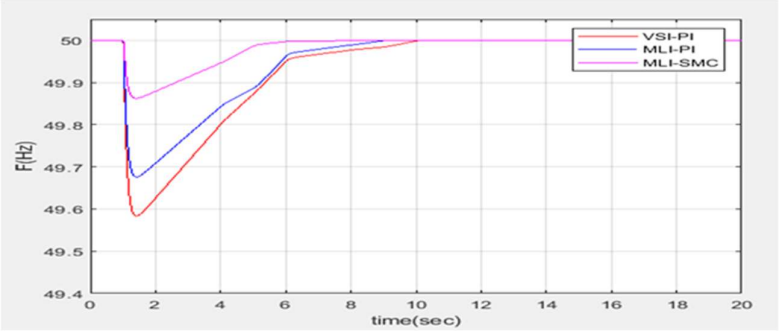

Figure 12: Frequency Response for Change in Load

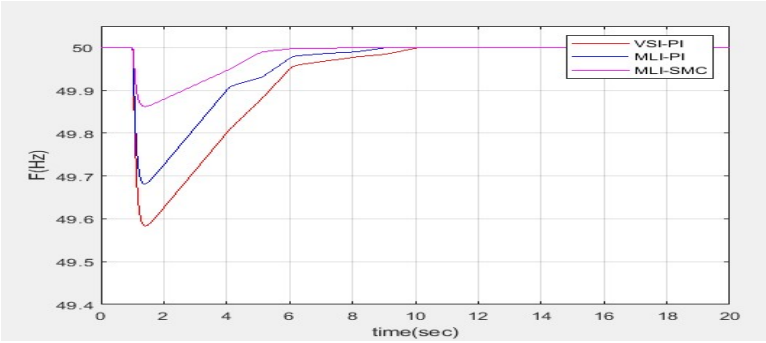

Figure 13: Frequency Response for Change in Load

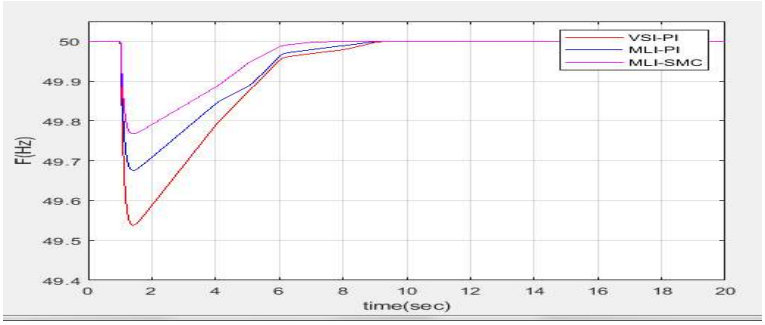

Figure 14: Frequency Response for Change in Load

First, we'll think about secondary regulation being performed by an SG representing a dynamic grid with constants of inertia with a time constant of 4 s, a fall rate of 5%, and an integral of 0.1 pu, the formula for this effect is H = R + KI. Together, the SG and GFC add 90MW to the electrical system. As can be seen in Fig. 16, there is a frequency shift as the load increases from 104 MW to 108 MW at time t = 1 s. At t = 1 s, the frequency of the grid decreases to 49.5 Hz but recovers thanks to secondary regulation services and returns to normal at t = 15 s. For this FFR tactic, the droop constant is set to R
= 0.05 pu, which is the same value used for the grid's droop constant.

GFC grid-active power response to changing loads from a variety of DC sources.

Figures 17–19 show the GFC's voltage response to different direct current (DC) sources and evaluated following a change in grid load. There is a gradual decrease in power from its peak of 1680 kW as the frequency stabilizes from the various sources taken into account. The results of the various systems are virtually identical, as is evident.

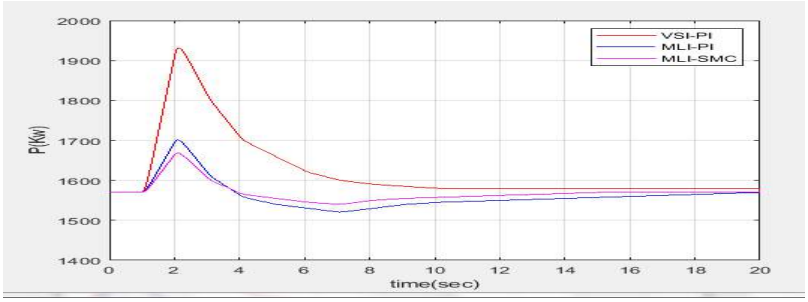

Figure 15: Battery

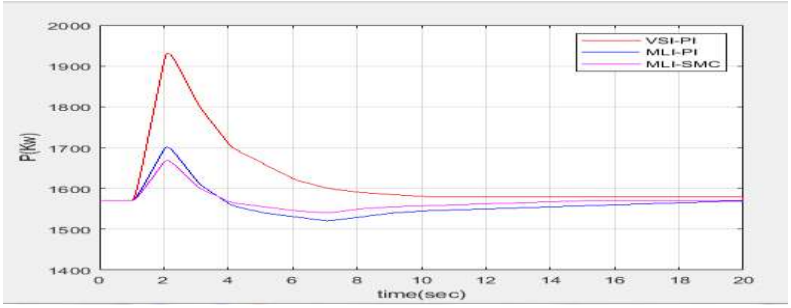

Figure 16: Wind Turbine

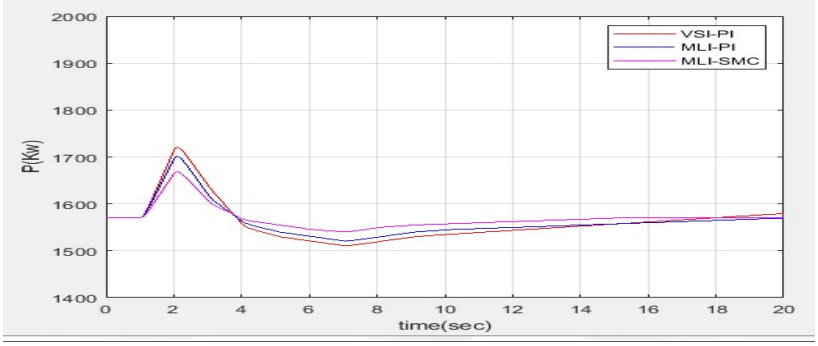

Figure 17: Solar

GFC the grid's reactive power response to a change in load for various DC sources Although the reference value is Q g = 0, Fig. 20-22 demonstrates how grid frequency changes are reflected in Qg, the reactive power, and keep it in sync. The lowest measured value of reactive power is 500 KVAr.

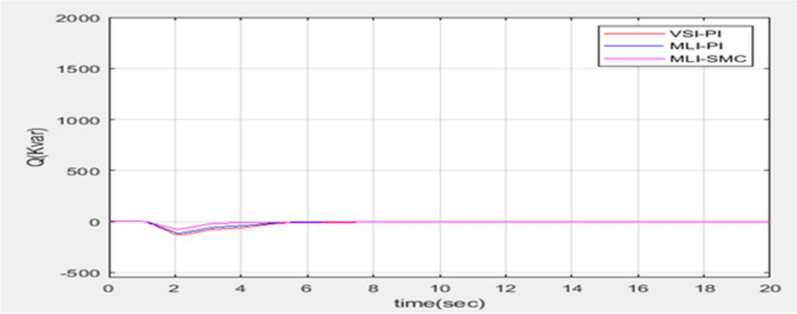

Figure 18: Battery

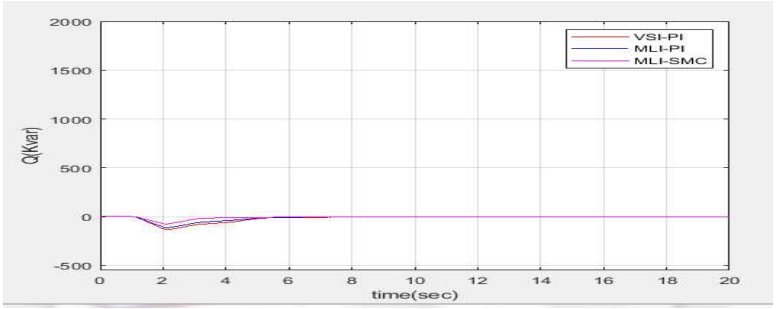

Figure 19: Wind Turbine

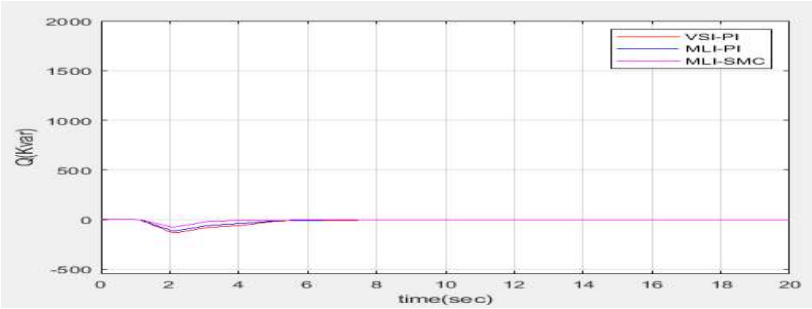

Figure 20: Solar

DC source voltage response to grid frequency shift.

All three DC voltage sources and their respective Vdc variations are shown in Figs. 23–25. The battery's voltage drops to 795 V due to the capacitive effect after a sharp decrease in frequency, it quickly recovers and returns to its pre-t = 20 s level at t = 20 s. There is a similar drop in DC voltage behavior in the FC turbine, but its dynamics are more rapid. with the voltage going beyond 800 V throughout the voltage recovery phase before stabilizing at 20 seconds. It drops to 755 V for the PV plant but then surges to 800 V. As a result, there are occasions when the actual power output is less than the one expected.

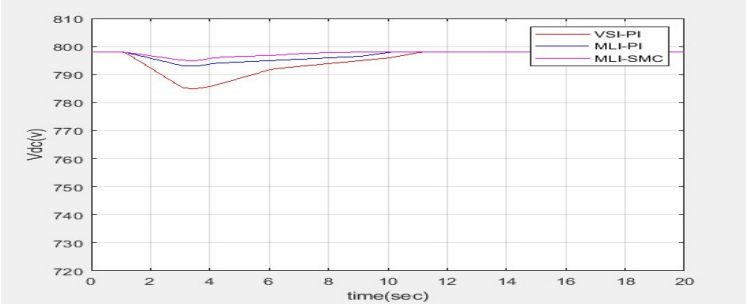

Figure 21: Battery

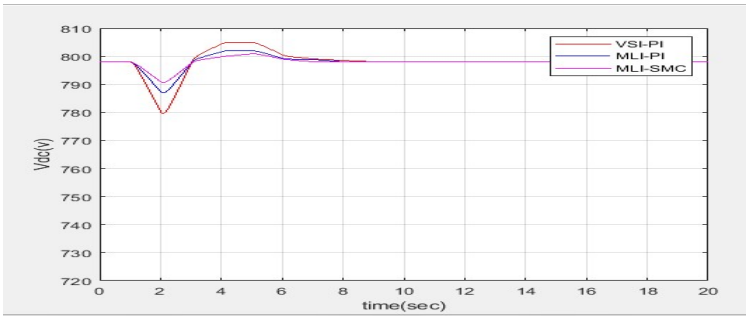

Figure 21: Wind Turbine

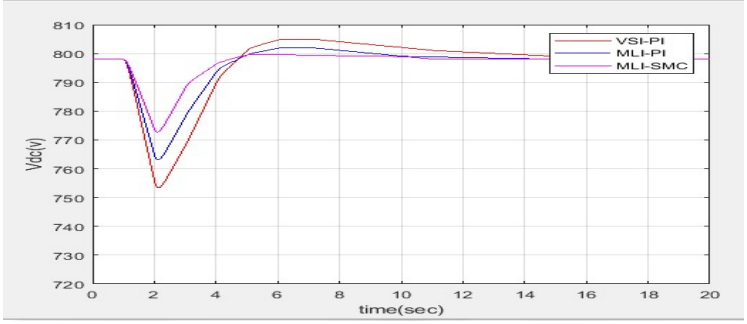

Figure 22: Solar

Case-2:

When the GFC is linked to the grid, the AC voltage is regulated by the RPS loop. From t = 0.5 s to t = 1.09 s, the GFC's response to an increase in terminal voltage from the grid is seen in Fig. 31. The GFC's droop control will be activated when the grid voltage increases, causing a drain of 1 MVAr. Despite the inclusion of Qg in the synchronization loop, this research reveals that the GFC may still assist in AC voltage management through the trading of reactive power. Accurately regulating the AC voltage requires grid electricity to be drawn in a short circuit. Therefore, when the short-circuit ratio is large, a considerable volume of reactive power must be exchanged in order to adjust the voltage at the GFC terminals.

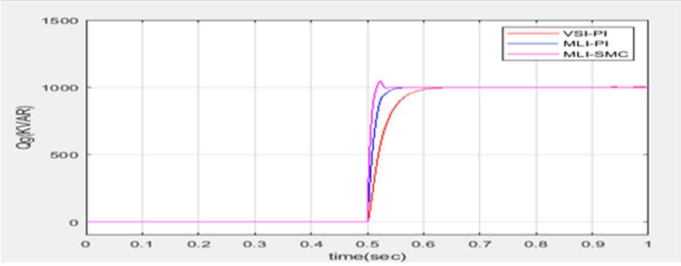

Figure 23: Response of the GFC's reactive power to an increase in alternating current voltage

Case.3:

GFCs are required to meet certain conditions when used as voltage sources, It can function both on the mains and independently, depending on the situation. Significant voltage and frequency changes can occur at the converter terminals when a converter transitions from grid-following to islanded mode, especially when a dynamic load is applied. We discuss the GFC's dynamic response under the hot-swapping control approach after a grid disconnection at t = 0:5 s with the converter supplying a dynamic load.

As vq is held constant at 0 by the RPS block, the GFC is synchronized with the grid. In order to keep the V* reference in sync with the real voltage of the grid (vd =1 pu), the vd voltage regulator must also be on and operating with an integrator time constant of T =0.3 s. The rated voltage is 1.05 pu, but the Vref voltage has been set higher. With a constant current of i dhs=0 and a voltage of 0.05 pu, we have a steady state. At t = 0:5 s, the main switch (s1) will trip, and the resulting voltages (vd and vq) are depicted in Fig. 33.

When the grid is cut off, the voltage across the capacitor drops quickly, prompting the voltage

regulator, vd;, to inject the current, i dhs 0. The increase in the reference voltage, Vref, The above procedure is carried out exactly to adjust dropping voltage right after a switch trips. At Vref = 2 s, the voltage increases from the low of 0.9 pu in Fig. 33 to a high of 1.05 pu. The instantaneous reactive power ripple will cause the grid frequency to oscillate at roughly 50 Hertz before the switch trips. However, when the GFC performs a hot swap into islanded mode following a disconnect, the control system imposes a frequency of exactly 50 Hz. When both the active and reactive power outputs are zero, the switch will trip, and the frequency (1!) will be equal to zero. Fig. 33 depicts the frequency as it appears at the converter's output terminals. The converter's output voltage has the standard pulse width modulation profile. The instantaneous voltage, va, is slightly distorted due to a discontinuity in the commutation observed when the switch trips.

In isolated mode, the GFC adjusts voltage and frequency and produces only active and reactive power to run the load. Fig. 35 depicts the shift from grid-connected to island-operated motor supply as a function of converter active power P and grid power Pg. The grid supplies the load's active power (1 MW) while the GFC power setpoint is zero, and then the switch trips. When the switch is thrown, grid power is cut off (Pg = 0), and the GFC takes over the motor load, with its power oscillating due to voltage fluctuations.

Reactive power (Q) is plotted against time as it is output by the converter in Fig. 31. (t). The value of Qg, the reference reactive power, is constant. If the frequency is slightly off from 50 hertz, as shown in Fig. 23, Qg will rise slightly before the switch trips. Q, the reactive power required by the motor minus the power stored in the filter capacitors, is provided by the converter. The GFC's reactive power will oscillate once it is cut off from the grid because of the momentary voltage fluctuations at the terminals. The oscillation is dampened at time t = 2 s, and Q does not change until the switch trips.

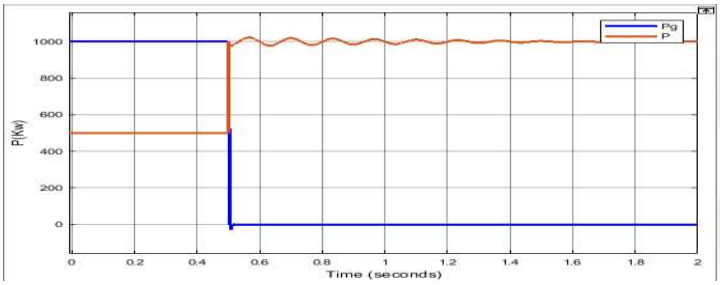

Figure 24: Power consumed from the grid, denoted by Pg, and power produced by the GFC, denoted by P

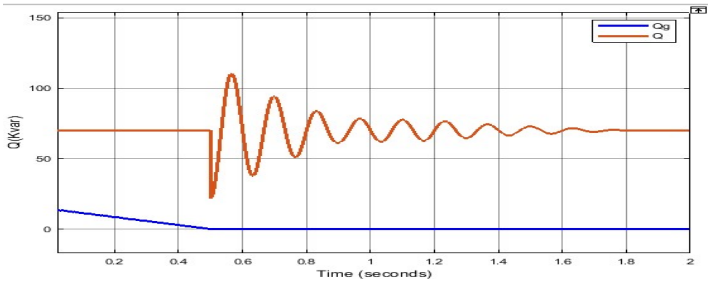

Figure 25: Reactive power drawn of the grid, Qg and reactive power generated by the GFC,

Q

Table-1: Comparison of Time domain specifications for different DC Sources used in the study for different Control Strategies

BATTERY

	Rise time	Peak time	Delay time	Settling time
VSC + PI	2.5 SEC	3.2 SEC	2 SEC	11 SEC
MLI + PI	2.4 SEC	2.8 SEC	2 SEC	10 SEC
MLI + SMC	2.3 SEC	2.7 SEC	2 SEC	8.5 SEC

WIND TURBINE

	RISE TIME	PEAK TIME	DELAY TIME	SETTLING TIME
VSC + PI	2.5SEC	3.2 SEC	2 SEC	11 SEC
MLI + PI	2.2 SEC	2.7 SEC	2 SEC	10.2 SEC
MLI + SMC	2.1 SEC	2.6 SEC	2 SEC	9 SEC

SOLAR

	RISE TIME	PEAK TIME	DELAY TIME	SETTLING TIME
VSC + PI	2.5 SEC	3 SEC	2 SEC	10 SEC
MLI + PI	2.3 SEC	2.8 SEC	2 SEC	10 SEC
MLI +SMC	2.1 SEC	2.6 SEC	2 SEC	8.8 SEC

Table-2: Parameters used for Li -ion Battery

PARAMETER	**VALUE**
Maximum Voltage	900 V
Nominal Voltage	800 V
Minimum Voltage	600 V
Exponential Voltage	825 V
Nominal Capacity	1300 Ah
Exponential Capacity	100 Ah
Battery Constant Voltage	858 V
Polarization Voltage	38.5 Ah
Exponential zone Amplitude	81 V
Exponential zone time Constant Inverse	0.03 /Ah
Internal Resistance	16 milli ohms
Capacitance	85 F

Table-3: parameters used for PV Panel

PARAMETER	**VALUE**
Maximum Power	2000 KW
Maximum Power Voltage	700V
Open circuit voltage	872 V

Short circuit current	3098 A
Series Resistance	5.88 ohms
Parallel Resistance	11 kilo ohms
Norton Impedance	29.75 ohms
DC Capacitance	150 mF
Number of modules in series	27
Number of strings in Parallel	370

Table-4: parameters used in the study

PARAMETER	VALUE (PU)
Converter Rated Power	1.00
Line to Line Rated Voltage	1.00
Filter Inductance	0.149
Filter Resistance	0.005
Filter Capacitance	0.150
Nominal Frequency	1.00
Switching Frequency	60
Synchronization Constant	0.03
Grid Inductance	0.019
Grid Resistance	0.002
Short Circuit ratio	50
X/R Ratio	10
Motor Rated Power	1.00
Phase Rated Voltage	1.00
Stator Resistance	0.074
Rotor resistance	0.025
Stator Winding Leakage	0.032
Rotor Winding Leakage	0.032
Magnetizing Inductance	2.946
Number of Poles	4
Moment of Inertia	50 kg/m^2
Inertia Constant	0.6 sec

V. CONCLUSIONS

These results motivate us to propose a novel GFC control system built on the RPS method for usage with renewable energy sources like as photovoltaic (PV) generators, fluid-dynamic (FC) wind turbines, and batteries. As a first step, we provide an overview of the RPS method and discuss the instantaneous active and reactive powers as well as the transfer function between Qg and in terms of their dynamic coupling. The main advantage of this technology is that it allows for efficient integration of the many generation sources that are connected to the DC input bus by decoupling the active power control and synchronization loops. This study also proposes the usage of Multi level Inverters in order to reduce the harmonics and increase the

magnitude of voltage and power when compared to voltage source converter. This study also proposes the usage of sliding mode control against the traditional PI Controller in order improve the time domain specifications like settling time and also reduces the steady state error.

REFERENCES

[1] JOSÉ LUIS RODRÍGUEZ AMENEDO, (Senior Member, IEEE), SANTIAGO ARNALTESGÓMEZ, JAIME ALONSO-MARTINEZ , AND MARCIAL GONZÁLEZ DE ARMAS , " Grid- Forming Converters Control Based on the Reactive Power Synchronization Method for Renewable Power Plants"in PROMINT-CM under Project S2018/EMT-4366. May 13 2021

[2] R. H. Lasseter, ''Microgrids,'' in Proc. IEEE Power Eng. Soc. Winter Meeting Conf., vol. 1, Jan. 2002, pp. 305–308.

[3] P. Rodriguez, ''Control of power converters in AC microgrids,'' IEEE Trans. Power Electron., vol.27, no. 11, pp. 4734–4749, Nov. 2012.

[4] P. Christensen, G. K. Andersen, M. Seidel, S. Bolik, S. Engelken, T. Knueppel, A. Krontiris, K. Wuerflinger, T. Bülo, J. Jahn, and M. Ndreko, ''High penetration of power electronic interfaced powersources and the potential contribution of grid forming converters,'' ENTSO-E, Brussels, Belgium, Tech. Rep. 1, 2020.

[5] Establishing a Network Code on Requirements for Grid Connection of Generators, Commission Regulation (EU) 2016/631, Brussels, Belgium, 2016.

[6] N. Hatziargyriou, ''Task force on definition and characterization of dynamic behavior in systems with high penetration of power electronic interfaced technologies,'' Power Energy Soc., Piscataway, NJ, USA, Tech. Rep. PES-TR77, 2020.

[7] B. Yu, M. Matsui, and G. Yu, ''A review of current anti-islanding methods for photovoltaic powersystem,'' Sol. Energy, vol. 84, no. 5, pp. 745–754, May 2010.

[8] R. Teodorescu, M. Liserre, and P. Rodriguez, Grid Converters for Photovoltaic and Wind Power Systems, vol. 29. Hoboken, NJ, USA: Wiley, 2011.

[9] A. Luna, J. Rocabert, J. I. Candela, J. R. Hermoso, R. Teodorescu, F. Blaabjerg, and P. Rodriguez,''Grid voltage synchronization for distributed generation systems under grid fault conditions,'' IEEE Trans. Ind. Appl., vol. 51, no. 4, pp. 3414–3425, Jul. 2015.

[10] M. Karimi-Ghartemani, ''A unifying approach to single-phase synchronous reference frame PLLs,'' IEEE Trans. Power Electron., vol. 28, no. 10, pp. 4550–4556, Oct. 2013.

[11] X. Wang and F. Blaabjerg, ''Harmonic stability in power electronic-based power systems: Concept, modeling, and analysis,'' IEEE Trans. Smart Grid, vol. 10, no. 3, pp. 2858–2870, May 2019.

[12] M. G. Taul, X. Wang, P. Davari, and F. Blaabjerg, ''An overview of assessment methods for synchronization stability of grid-connected converters under severe symmetrical grid faults,'' IEEE Trans. Power Electron., vol. 34, no. 10, pp. 9655–9670, Oct. 2019.